Appendix A: Detailed description of data, MAR modeling and data transformation

Data collection

Thirty photoquadrats (1 x 1 m) were recorded annually at Tektite and Yawzi Point, and 108-240 photoquadrats (0.5 x 0.5 m) were recorded at the RS (the RS sample size was increased in 2000 with the application of digital photography). Percentage cover of each group was determined using the software CPCe (Kohler & Gill 2006) with 200 randomly located dots on each image. A map of all study locations can be found in Edmunds (2013). Annual cover composition at each of the six sites that comprise the RS data are shown in Fig. A1.

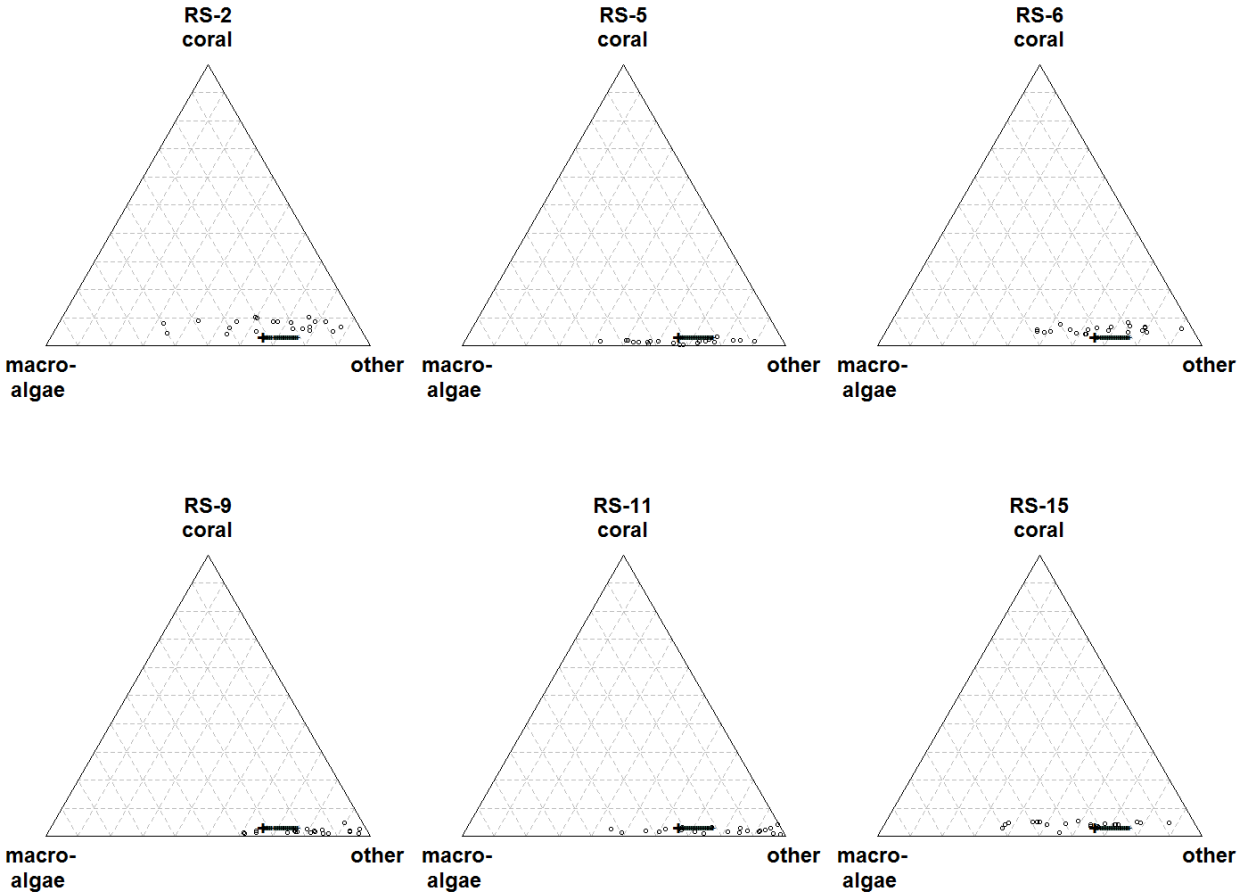

Figure A1. Composition of coral cover, macroalgal cover, and 'other' for the six sites that comprise the RS data. Site labels correspond to designations from Edmunds (2013). Large plus (+) symbols show the metric center of the quasi-stationary distribution for 2012, and small plus symbols trace how this mean has changed from 1992 – 2012. Open circles symbols show annual compositions.

Vectors and matrices in MAR model

For the cover analysis, the vectors and matrices in the MAR model (eq. 1) have the following forms:

$$\mathbf{x}_t = \begin{bmatrix} x_1 \\ x_2 \end{bmatrix}_t ; \ \mathbf{a} = \begin{bmatrix} a_1 \\ a_2 \end{bmatrix}; \ \mathbf{B} = \begin{bmatrix} b_{11} & b_{12} \\ b_{21} & b_{22} \end{bmatrix}; \ \mathbf{C} = \begin{bmatrix} c_{11} & c_{12} \\ c_{21} & c_{22} \end{bmatrix}; \ \mathbf{z} = \begin{bmatrix} z_1 \\ z_2 \end{bmatrix}; \ \mathbf{u}_t = \begin{bmatrix} u_1 \\ u_2 \end{bmatrix}_t ; \ \mathbf{e}_t = \begin{bmatrix} \varepsilon_1 \\ \varepsilon_2 \end{bmatrix}_t . \quad (1)$$

For the RS habitat, there is a unique intercept vector **a** for each of the six sites. For the taxonomic analysis, the vectors and matrices in the MAR model (eq. 1) have the following forms:

$$\mathbf{x}_t = \begin{bmatrix} x_1 \\ x_2 \\ x_3 \\ x_4 \\ x_5 \\ x_6 \end{bmatrix}_t ; \ \mathbf{a} = \begin{bmatrix} a_1 \\ a_2 \\ a_3 \\ a_4 \\ a_5 \\ a_6 \end{bmatrix}; \ \mathbf{B} = \begin{bmatrix} b_{11} & 0 & 0 & 0 & 0 & 0 \\ 0 & b_{22} & 0 & 0 & 0 & 0 \\ 0 & 0 & b_{33} & 0 & 0 & 0 \\ 0 & 0 & 0 & b_{44} & 0 & 0 \\ 0 & 0 & 0 & 0 & b_{55} & 0 \\ 0 & 0 & 0 & 0 & 0 & b_{66} \end{bmatrix}; \ \mathbf{C} = \begin{bmatrix} c_{11} & c_{12} \\ c_{21} & c_{22} \\ c_{31} & c_{32} \\ c_{41} & c_{42} \\ c_{51} & c_{52} \\ c_{61} & c_{62} \end{bmatrix};$$

$$\mathbf{z} = \begin{bmatrix} z_1 \\ z_2 \\ z_3 \\ z_4 \\ z_5 \\ z_6 \end{bmatrix}; \ \mathbf{u}_t = \begin{bmatrix} u_1 \\ u_2 \end{bmatrix}_t ; \ \mathbf{e}_t = \begin{bmatrix} \varepsilon_1 \\ \varepsilon_2 \\ \varepsilon_3 \\ \varepsilon_4 \\ \varepsilon_5 \\ \varepsilon_6 \end{bmatrix}_t . \quad (2)$$

For the RS habitat, there is a unique intercept vector **a** and a unique trend vector **z** for each of the six sites. The only parameters that are shared between the cover and taxonomic analyses are the mean vector $\boldsymbol{\mu}_u$ and variance matrix $\boldsymbol{\Sigma}_u$ for the environmental covariates. (This is because the values of the environmental covariates are the same for both cover and taxonomic analysis.) All other model parameters have separate values for the cover and taxonomic analysis.

Data transformation

In notation, if we write the proportional cover of coral, macroalgae, and 'other' as p_1, p_2, and p_3, respectively, then the corresponding isometric log-ratio (ilr) coordinates are

$$x_1 = \frac{1}{\sqrt{2}} \ln\left(\frac{p_1}{p_2}\right), \quad x_2 = \frac{2}{\sqrt{6}} \ln\left(\frac{\sqrt{p_1 p_2}}{p_3}\right). \tag{3}$$

With a change in sign, this is the same transformation used by Cooper et al. (*in press*). In short, ilr coordinates are orthogonal contrasts of the log proportions; results on the proportion scale do not depend on the particular set of contrasts chosen. Here, x_1 quantifies the difference between coral vs. macroalgae cover, and x_2 quantifies the difference between the geometric mean of coral and macroalgae cover vs. 'other'. This particular set of contrasts is based on a sequential binary partition (Egozcue and Pawlowsky-Glahn 2011; see their formula for 'balances' in their section 2.4). As Cooper et al. (*in press*) note, an ilr transformation is a sensible transformation for community compositions, because exponential growth of all components of the composition results in linear dynamics on the ilr scale (Egozcue et al. 2003). Time series of cover composition on the ilr-transformed scale are shown in fig. A2.

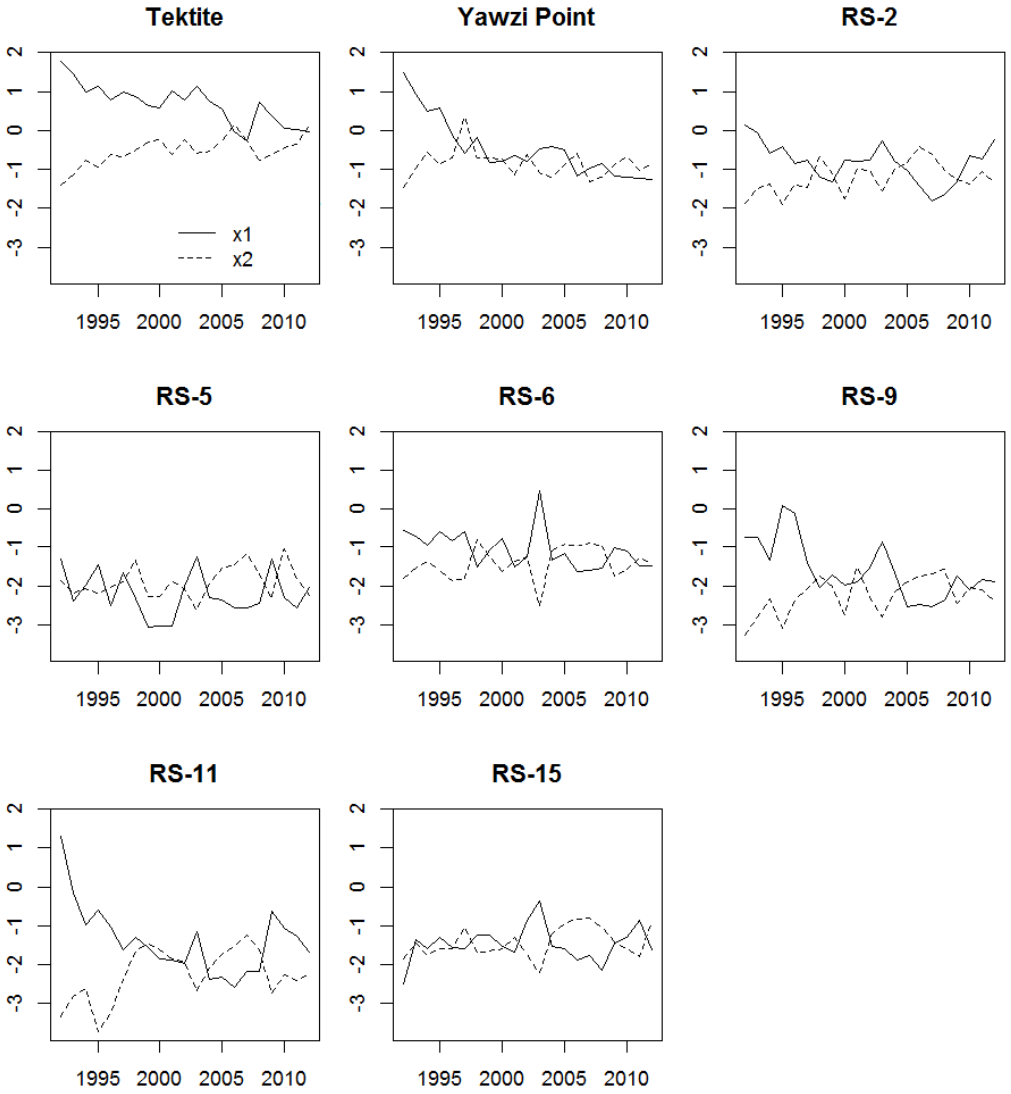

Figure A2. Cover composition in ilr coordinates for Tektite, Yawzi Point, and the 6 random sites.

To convert results back to the native proportion scale, write the cover proportions as the 3-vector **p**, write the ilr coordinates as the 2-vector **x**, and write the ilr transformation as $g()$, such that $\mathbf{x}=g(\mathbf{p})$ and $\mathbf{p}=g^{-1}(\mathbf{x})$. Applying the inverse transformation g^{-1} to $\boldsymbol{\mu}_{\mathbf{x}}$

$$\boldsymbol{\mu}_{\mathbf{p}}=g^{-1}(\boldsymbol{\mu}_{\mathbf{x}}) \tag{4}$$

yields the so-called “metric center” of the composition, which Aitchison (1989) and Pawlowsky-Glahn and Egozcue (2001) have argued provides the best measure of center for a composition. A linear approximations for the variance of the stationary distribution on the proportion scale (denoted $\mathbf{\Sigma}_p$) is simply

$$\mathbf{\Sigma}_p \approx \nabla g^{-1}(\boldsymbol{\mu}_x)\mathbf{\Sigma}_x \nabla g^{-1}(\boldsymbol{\mu}_x)^T \ . \tag{5}$$

Expressions for eq. (4)-(5) on the proportion scale follow from the chain rule of calculus:

$$\frac{d\boldsymbol{\mu}_p}{d\boldsymbol{\mu}_u} \approx \nabla g^{-1}(\boldsymbol{\mu}_x)(\mathbf{I}-\mathbf{B})^{-1}\mathbf{C}; \quad \frac{d\boldsymbol{\mu}_p}{dt^*} \approx \nabla g^{-1}(\boldsymbol{\mu}_x)(\mathbf{I}-\mathbf{B})^{-1}\mathbf{z}; \tag{6}$$

$$\frac{d\mathrm{Vec}(\mathbf{\Sigma}_p)}{d\mathrm{Vec}(\mathbf{\Sigma}_u)} \approx \left(\nabla g^{-1}(\boldsymbol{\mu}_x) \otimes \nabla g^{-1}(\boldsymbol{\mu}_x)\right)(\mathbf{I}-\mathbf{B}\otimes\mathbf{B})^{-1}(\mathbf{C}\otimes\mathbf{C}) \ . \tag{7}$$

Literature cited in Appendix A

Aitchison, J. 1989. Measures of location of compositional data sets. Mathematical Geology 21:787 – 790.

Cooper, J.K., M. Spencer, and J. F. Bruno. Stochastic dynamics of a warmer Great Barrier Reef. Ecology, *in press*.

Edmunds, P. J. 2013. Decadal-scale changes in the community structure of coral reefs of St. John, US Virgin Islands. Marine Ecology Progress Series 489:107–123.

Egozcue, J. J., and V. Pawlowsky-Glahn. 2011. Basic concepts and procedures. Pages 12–28 *in* V. Pawlowsky-Glahn and A. Buccianti, editors. Compositional data analysis: theory and applications. John Wiley and Sons New York, NY.

Egozcue, J. J., V. Pawlowsky-Glahn, G. Mateu-Figueras, and C. Barcelo-Vidal. 2003. Isometric logratio transformations for compositional data analysis. Mathematical Geology 35:279–300.

Kohler, K. E., and S. M. Gill. 2006. Coral Point Count with Excel extensions (CPCe): A Visual Basic program for the determination of coral and substrate coverage using random point count methodology. Computers & Geosciences 32:1259–1269.

Pawlowsky-Glahn, V., and J. J. Egozcue. 2001. Geometric approach to statistical analysis on the simplex. Stochastic Environmental Research and Risk Assessment 15:384–398.

Appendix B: Mathematical proofs of equations (2) and (3)

Fix time *t* at t^*. Re-write eq. (1) as

$$\mathbf{x}_t = \mathbf{a} + \mathbf{z}t^* + \mathbf{C}\boldsymbol{\mu}_\mathbf{u} + \mathbf{B}\mathbf{x}_{t-1} + \mathbf{C}\mathbf{u}_t - \mathbf{C}\boldsymbol{\mu}_\mathbf{u} + \mathbf{e}_t \qquad t = 2,3,....$$

Set the constant $\mathbf{a} + \mathbf{z}t^* + \mathbf{C}\boldsymbol{\mu}_\mathbf{u}$ equal to $\tilde{\mathbf{a}}$, and set the random sum $\mathbf{C}\mathbf{u}_t - \mathbf{C}\boldsymbol{\mu}_\mathbf{u} + \mathbf{e}_t$ equal to $\tilde{\mathbf{e}}$. Note that the expectation of $\tilde{\mathbf{e}}$ is $\mathrm{E}\left[\mathbf{C}\mathbf{u}_t - \mathbf{C}\boldsymbol{\mu}_\mathbf{u} + \mathbf{e}_t\right] = \mathbf{C}\boldsymbol{\mu}_\mathbf{u} - \mathbf{C}\boldsymbol{\mu}_\mathbf{u} = \mathbf{0}$, and the variance of $\tilde{\mathbf{e}}$ is $\mathrm{Var}\left[\mathbf{C}\mathbf{u}_t - \mathbf{C}\boldsymbol{\mu}_\mathbf{u} + \mathbf{e}_t\right] = \mathbf{C}\boldsymbol{\Sigma}_\mathbf{u}\mathbf{C}^T + \boldsymbol{\Sigma}_\mathbf{e}$ (recall that $\mathbf{u}_t$ and $\mathbf{e}_t$ are assumed independent). Thus, eq. (1) can be re-written as

$$\mathbf{x}_t = \tilde{\mathbf{a}} + \mathbf{B}\mathbf{x}_{t-1} + \tilde{\mathbf{e}}_t \qquad t = 2,3,....$$

which is the multivariate AR(1) model from Ives et al. (2003) (their eq. 10). Thus, the mean and variance of the stationary distribution follow immediately as

$$\begin{aligned}\boldsymbol{\mu}_\mathbf{x} &= \left(\mathbf{I} - \mathbf{B}\right)^{-1}\tilde{\mathbf{a}} \\ &= \left(\mathbf{I} - \mathbf{B}\right)^{-1}\left(\mathbf{a} + \mathbf{C}\boldsymbol{\mu}_\mathbf{u} + \mathbf{z}t^*\right)\end{aligned}$$

and

$$\begin{aligned}\mathrm{Vec}\left(\boldsymbol{\Sigma}_\mathbf{x}\right) &= \left(\mathbf{I} - \mathbf{B}\otimes\mathbf{B}\right)^{-1}\mathrm{Vec}\left(\mathrm{Var}\left(\tilde{\mathbf{e}}\right)\right) \\ &= \left(\mathbf{I} - \mathbf{B}\otimes\mathbf{B}\right)^{-1}\mathrm{Vec}\left(\mathbf{C}\boldsymbol{\Sigma}_\mathbf{u}\mathbf{C}^T + \boldsymbol{\Sigma}_\mathbf{e}\right).\end{aligned}$$

Appendix C: Residual diagnostics and analysis for cover and taxonomic models

The figures in this appendix show diagnostic plots for residuals from the cover analysis (Figs. C1 – C2) and the taxonomic analysis (Figs. C3 – C4). The MAR model assumes that the vector-valued residuals are serially independent and identically distributed. Thus, residual plots such as these are useful for diagnosing whether or not the variance of the residuals changes with time, or is different for large or small fitted values.

Few features stand out in the residual plot for the cover analysis, except for perhaps the occasional residual with a very large absolute value. Residuals from the taxonomic analysis seem do occasionally demonstrate banding characteristic of log-transformed data for that is below the limit of detection. For example, *Montastrea* was not observed at site RS-5 for 1992 – 2004, and was only detected at small densities in three of the years thereafter. Such banding suggests that, for those coral genera that were frequently below the detection limit from one or more sites (namely, *Montastrea*), sensitivities to hurricanes and sea temperature may be near zero simply because environment will have no observed impact on the growth rates of an undetected coral.

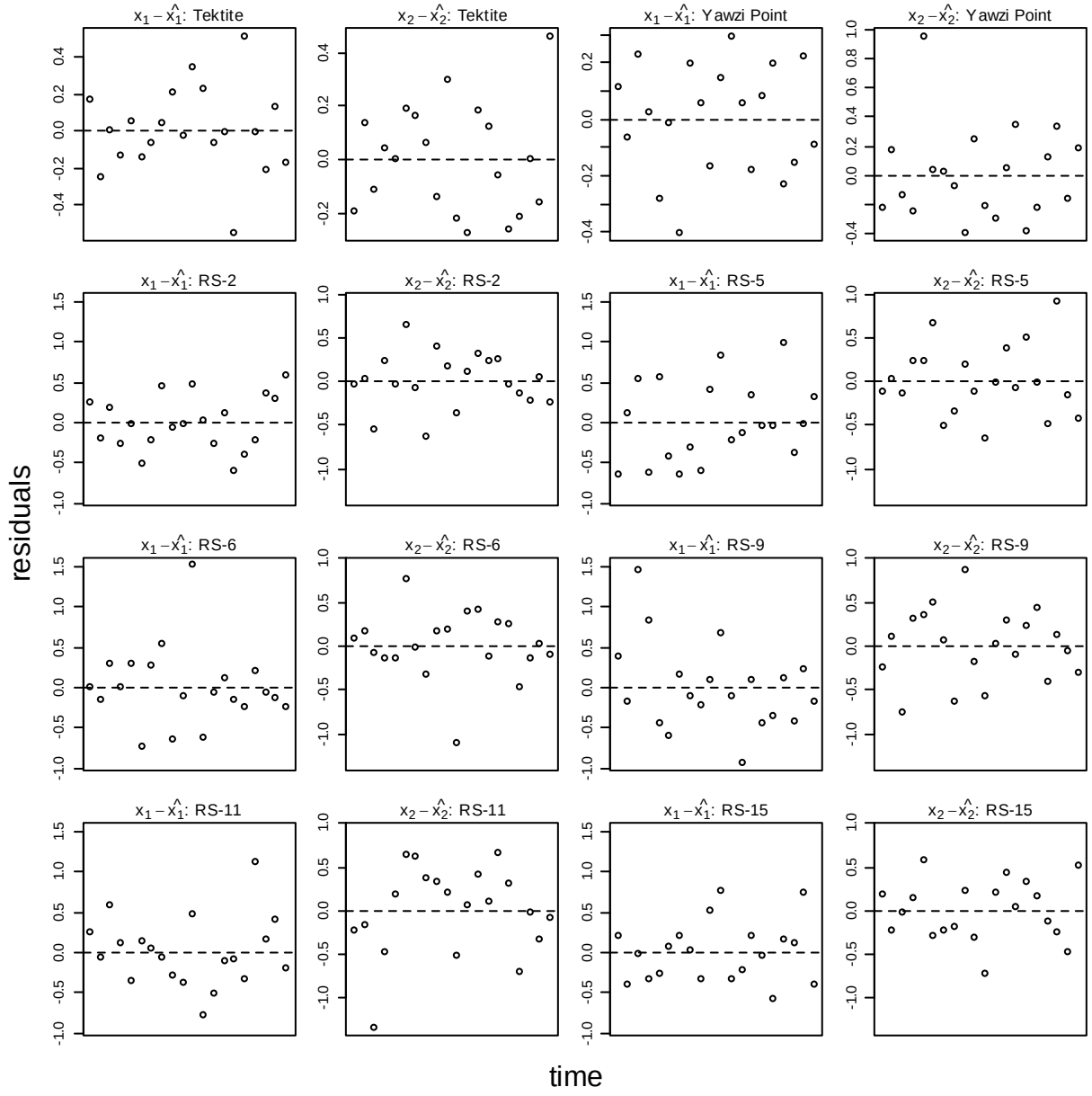

Figure C1. Plots of residuals vs. time for ilr-transformed compositions at Tektite, Yawzi Point, and the random sites.

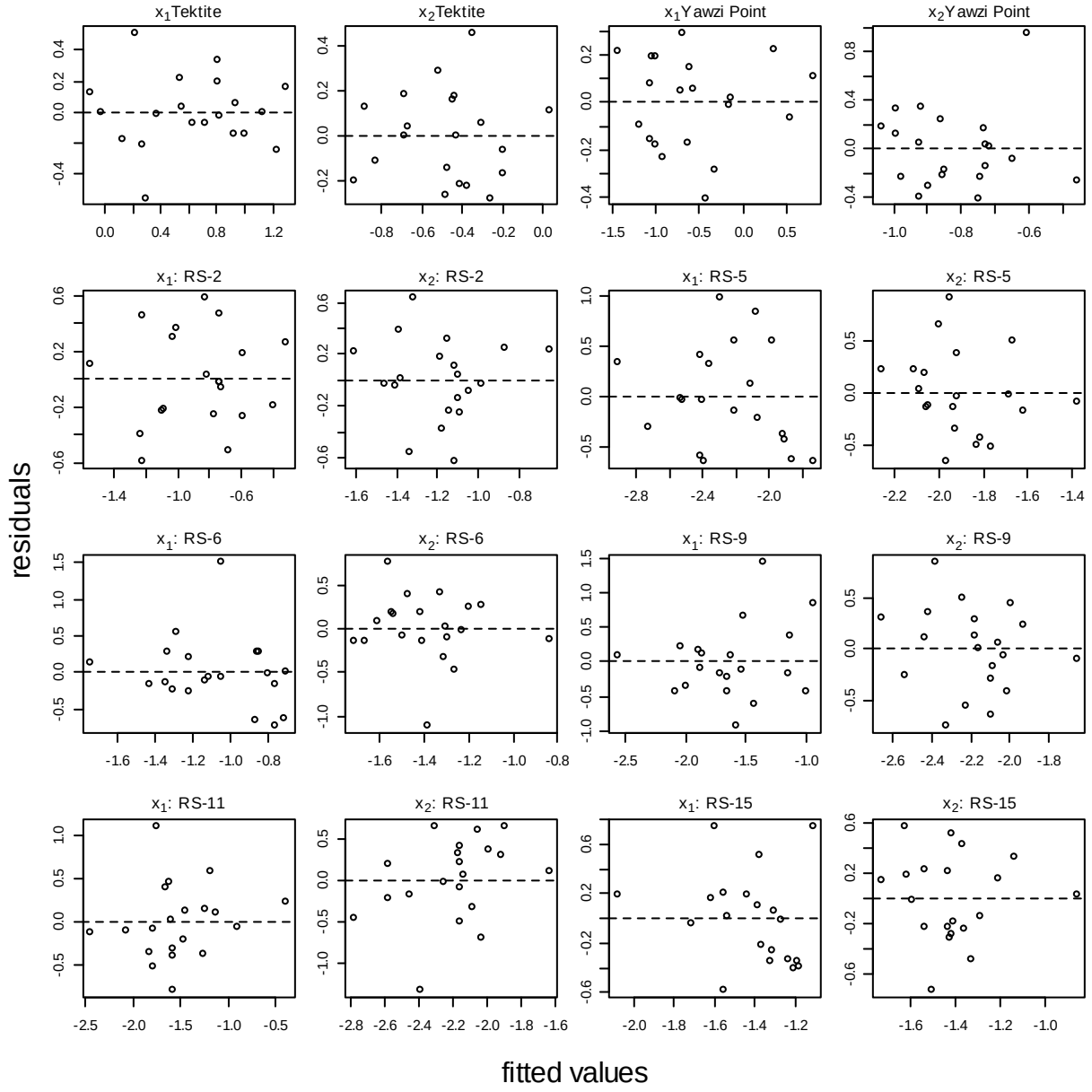

Figure C2. Plots of residuals vs. fitted values for ilr-transformed compositions at Tektite, Yawzi Point, and the individual random sites.

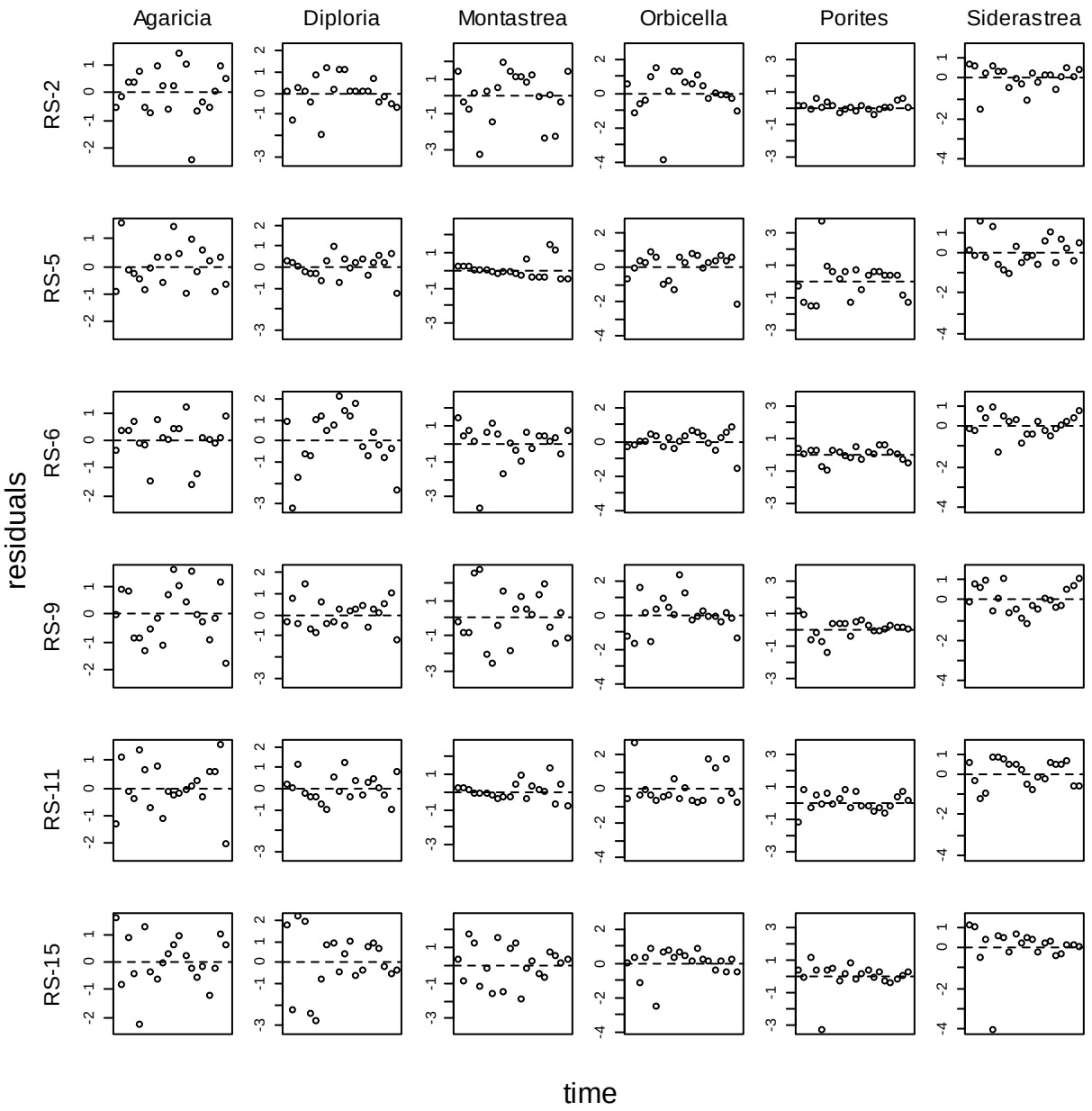

Figure C3. Plots of residuals vs. time for coral genera at individual random sites.

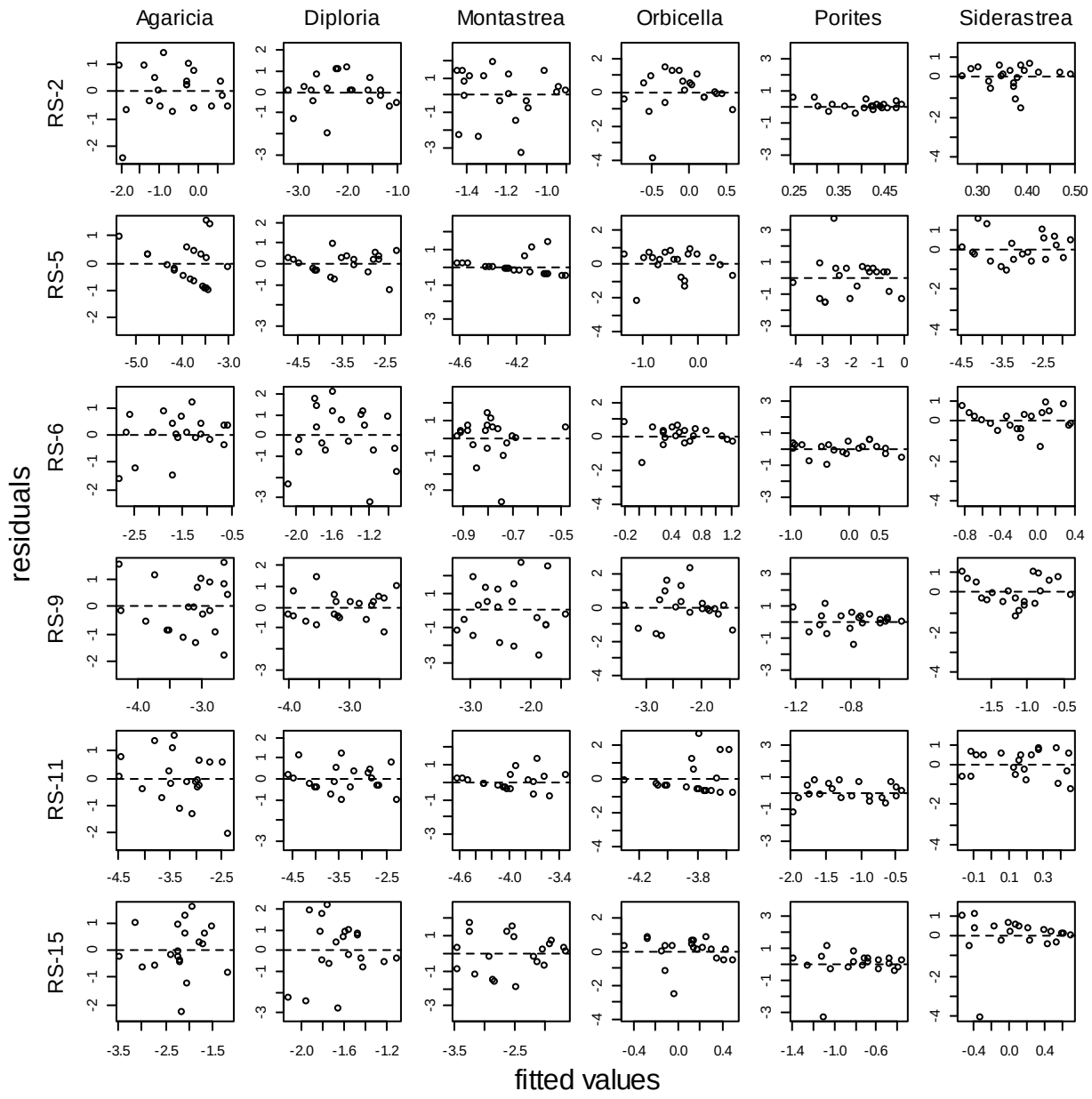

Figure C4. Plots of residuals vs. fitted values for coral genera at individual random sites.

Appendix D: Simulation studies of small-sample properties of MAR estimators

Simulation study 1: Sampling distributions of MAR model parameters and stability metrics under different magnitudes of trend

We conducted a small simulation study to investigate whether the trend covariate in eq. (1) impacted the estimation of several of the stability metrics calculated in the cover analysis. For each of the three habitats, we simulated data sets using the estimated values of **a**, **B**, and **C** in eq. (1) as the generative model. For the RS habitat, we used the average estimate of **a** across all sites. We simulated environmental variation and residual variation by sampling with replacement from the observed environmental vectors and the estimated residual vectors, respectively. Because our simulation focused on the effect of time, we ran simulations where **z** in the generative model equaled $k\mathbf{z}$, where k is a multiplier that diminished or amplified the trend by a factor of k=0, 0.5, 1, 1.5 or 2, and **z** equaled its estimated value. We refer to the k as the "trend multiplier". Initial values for the cover composition were drawn from the estimated quasi-stationary distribution for the first year of our study. Thus, we had 15 total simulation scenarios (three habitats crossed with five values of k). We simulated 1000 data sets for each simulation scenario, with each data set lasting for 21 time steps (the same duration as the actual data). Rare simulations that generated an estimated **B** matrix with a spectral radius greater than 1 were discarded. We report the mean, interquartile range, and 10^{th} and 90^{th} percentiles of the empirical sampling distribution for several model parameters and derived stability metrics.

Figure D1 shows the empirical sampling distribution for the elements of **a**, **B**, **C**, and **z** for each habitat and each value of *k*, along with actual values from the generative models. Not surprisingly, estimators are biased. This bias is not surprising because it is known that the conditional least-squares estimators of autoregressive models are only asymptotically unbiased, and will be biased for short time series. The key feature of figure D1, however, is that the marginal sampling distribution of the elements of **a**, **B**, and **C** do not appear to depend on the value of *k*. The standard error of the elements of **z** increases as *k* increases, but any bias in the elements of **z** appears to be small.

Figure D2 shows the empirical sampling distribution of several derived metrics for the same simulation scenarios. Results suggest varying degrees of bias in derived quantities, although the magnitude of the bias only depends minimally on the strength of the trend. Means of the quasi-stationary distribution — either on the ilr-transformed scale or on the proportion scale — show negligible bias. The CV of proportional coral cover at the quasi-stationary distribution is slightly downwardly biased for the Tektite scenario, and slightly upwardly biased for the RS. Sensitivities of mean coral cover (again, on the proportion scale) to both environmental covariates and the trend all seem to be estimated with little or negligible bias.

The spectral radius of the **B** matrix is biased for all simulation scenarios for Tektite and Yawzi Point, and in these cases is negatively biased (that is, the true spectral radius is larger than the average estimated spectral radius). That the spectral radius is estimated with bias is perhaps not surprising, given the strong non-linearity inherent in calculating eigenvalues.

Nevertheless, the bias makes it clear that differences between spectral radii across habitats (fig. 2b of the main text) should be interpreted cautiously.

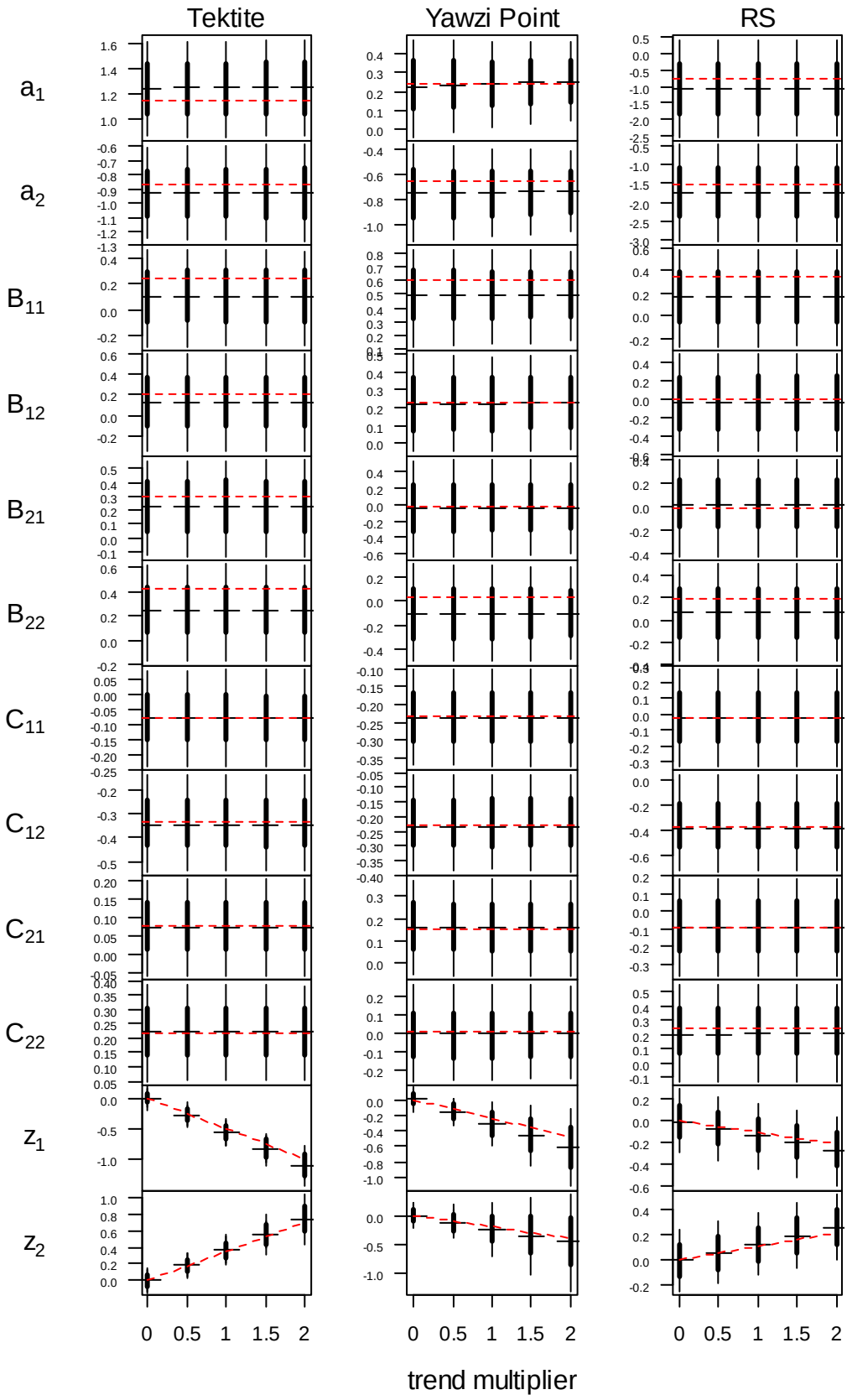
Tektite
Yawzi Point
RS
a1
a2
B11
B12
B21
B22
C11
C12
C21
C22
z1
z2
0
0.5
1
1.5
2
trend multiplier

*Figure D1 (previous page). Sampling distributions of the elements of **a**, **B**, **C**, and **z** for different simulated scenarios. Columns of panels correspond to the habitat that was used as the generative model, rows of panels show different parameters, and segments within panels show different values of the trend multiplier. Horizontal hashes show the average parameter estimate, thick vertical line segments span the interquartile range of the sampling distribution, and thin vertical line segments range from the 10^{th} percentile to the 90^{th} percentile of the sampling distribution. Red lines connect actual parameter values from the generative model.*

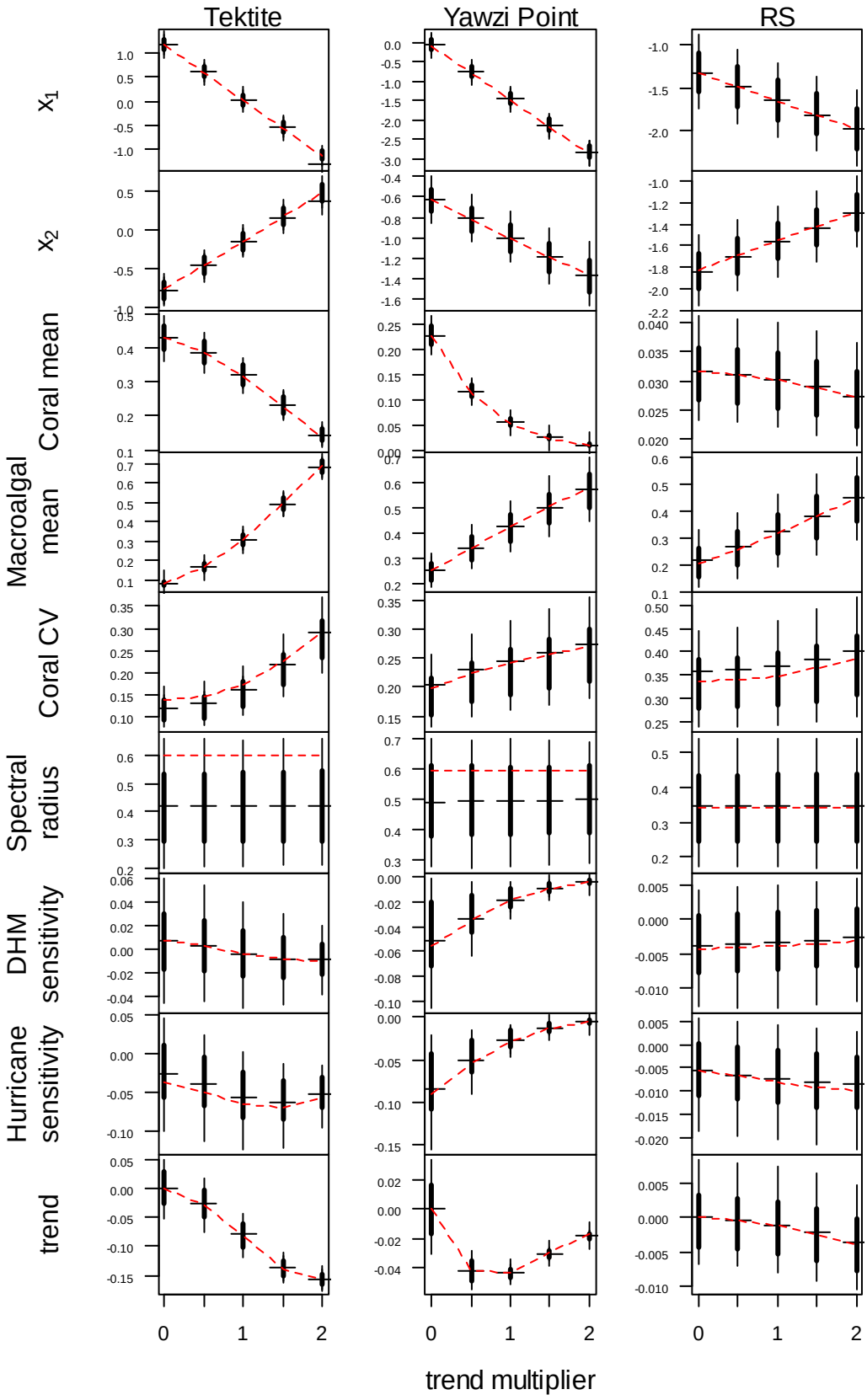
Tektite
Yawzi Point
RS
x_1
x_2
Coral mean
Macroalgal mean
Coral CV
Spectral radius
DHM sensitivity
Hurricane sensitivity
trend
trend multiplier

Figure D2 (previous page). Sampling distributions of derived quantities of interest for different simulated scenarios. Basic arrangement of panels is the same as Figure D1. First two rows: elements of $\boldsymbol{\mu}_x$ *(quasi-stationary distribution on the ilr-transformed scale). Third and fourth rows: elements of* $\boldsymbol{\mu}_p$ *, mean coral and macroalgal cover at the quasi-stationary distribution on the proportion scale. Fifth row: CV of coral cover at the quasi-stationary distribution, on the proportion scale. Sixth row: spectral radius. Seventh and eight rows: Sensitivity of average coral cover to environmental covariates, on the proportion scale (*$d\boldsymbol{\mu}_p / d\boldsymbol{\mu}_u \times \left(1/\boldsymbol{\mu}_p\right)$*). Ninth row: Trend of average coral cover per year, on the proportion scale (*$d\boldsymbol{\mu}_p / dt^* \times \left(1/\boldsymbol{\mu}_p\right)$*).*

Simulation study 2: Quality of approximate probability contours in figure 2 when $\boldsymbol{u}_t$ *and* $\boldsymbol{e}_t$ *are not normally distributed.*

Neither the MAR model (eq. 1) nor any of our results (eqq. 2 – 5) require a normality assumption for either the environmental covariates in $\mathbf{u}_t$ or the random errors in $\mathbf{e}_t$. However, the approximate probability contours for the quasi-stationary distribution shown in Fig. 2 are based on the assumption that the quasi-stationary distribution is multivariate normal on the ilr-transformed scale, which in turn relies on a normality assumption for both $\mathbf{u}_t$ and $\mathbf{e}_t$. To assess the accuracy of the approximate probability contours when $\mathbf{u}_t$ and $\mathbf{e}_t$ are not normally distributed, we simulated 5000 years of dynamics for the Tektite and Yawzi Point habitat from eq. (1), fixing the trend covariate at its 2012 value, and drawing $\mathbf{u}_t$ from its observed distribution and independently drawing $\mathbf{e}_t$ from the estimated residuals from each model.

Simulations were initiated from the estimated metric center of each quasi-stationary distribution, and the first 100 years of dynamics were discarded as a burn-in. Both $\mathbf{u}_t$ and $\mathbf{e}_t$ were sampled as vectors, thus preserving correlations between environmental covariates, and between the residuals in $\mathbf{e}_t$. These simulated dynamics provide a visualization of the exact quasi-stationary distribution for these two habitats, assuming that the actual distributions of $\mathbf{u}_t$ and $\mathbf{e}_t$ are identical to their empirical distributions (Fig. D3). The proportion of simulated data points that fall within the 50%, 80% and 95% probability contours shown in Fig. 1 of the main text are: 55.9%, 82.5%, and 95.2%, respectively, for Tektite; 57.3%, 87.2% and 94.0%, respectively, for Yawzi Point; and 56.4%, 81.5% and 93.2%, respectively, for the RS . Figure D4 shows a quantile-quantile plot of the Mahalanobis distances for the simulated dynamics on the ilr-transformed scale vs. theoretical quantiles from a χ^2_2 distribution. (This plot is the multivariate analog of the familiar normal probability plot used in residual analysis.)

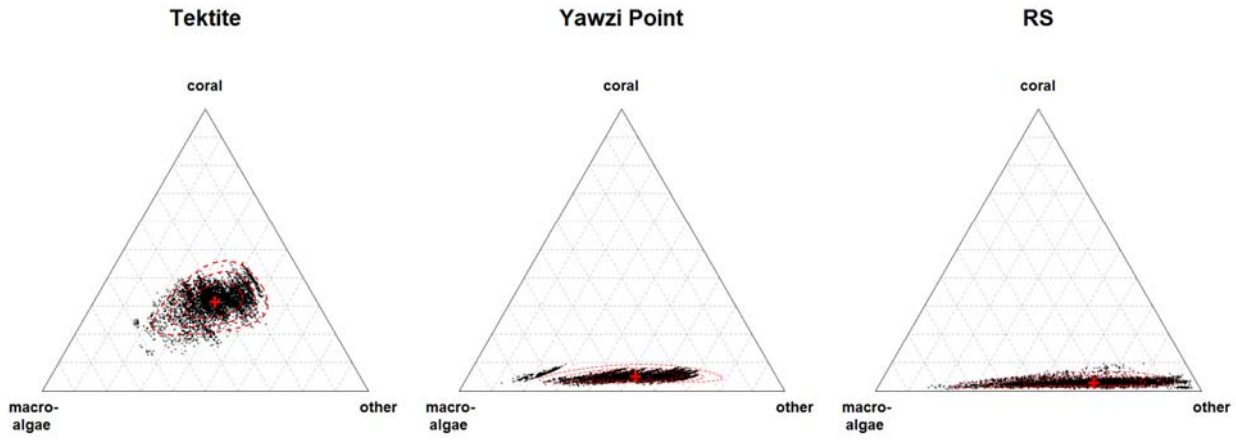

Figure D3. Triangle plots of 5000 years of simulated data from each of the three habitats, using the 2012 value of the trend covariate and the empirical distributions of $\mathbf{u}_t$ and $\mathbf{e}_t$. Red

dashed lines show approximate 50%, 80% and 95% probability contours for comparison, and are identical to those shown in Figure 1 of the main text.

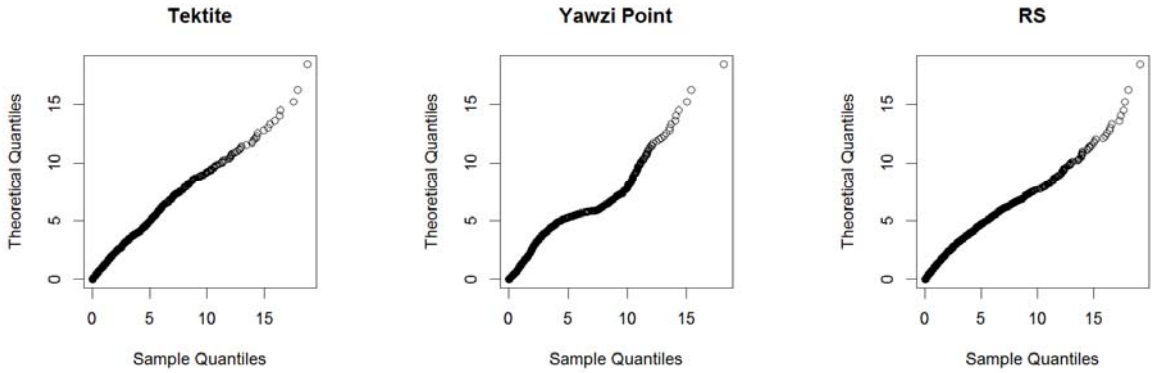

Figure D4. Quantile-quantile plots of the Mahalanobis distances of the simulated compositions (on the ilr-transformed scale) from the metric center of the quasi-stationary distribution for all three habitats, using a χ_2^2 *distribution for comparison. Departures from linearity suggest differences between the quasi-stationary distributions generated using empirical distributions of* $\boldsymbol{u}_t$ *and* $\boldsymbol{e}_t$ *(on the ilr-transformed scale) and their multivariate normal approximations.*

Taken together, these plots suggest that the approximate probability contours shown in Fig. 2 of the main text are reasonable approximations. There is some multimodality apparent in the distribution of simulated data at the Yawzi Point habitat, but this is likely a consequence of an anomalous residual (see Figure C1 of appendix C). This and other fine structure apparent in the empirical distribution of residuals is likely a consequence of the coarseness in the empirical distributions of $\mathbf{u}_t$ and $\mathbf{e}_t$ that arises from having a limited number of data points. It is unlikely that this coarseness would persist if more data were available. Thus, it seems appropriate to

view the normal-based probability contours as an approximation that captures the main features of the quasi-stationary distribution without over-fitting to idiosyncratic fine structure.

Appendix E: MAR model parameter estimates, full sensitivities for cover analysis, and sensitivities of variance of quasi-stationary distribution.

Tables E1 and E2 provide parameter estimates and robust bootstrap standard errors for the MAR parameters of the cover and taxonomic analysis, respectively. Parameter notation follows the detailed presentation in appendix A.

Table E1. Parameter estimates ± robust bootstrap standard errors for the cover analysis.

Parameter	Tektite	Yawzi Point	RS
a_1	0.65 ± 0.16	0.00 ± 0.25	-0.89 ± 0.50†
a_2	-0.52 ± 0.15	-0.85 ± 0.38	-1.42 ± 0.45†
b_{11}	0.25 ± 0.30	0.60 ± 0.19	0.34 ± 0.13
b_{12}	0.21 ± 0.29	0.22 ± 0.31	-0.01 ± 0.12
b_{21}	0.30 ± 0.36	-0.02 ± 0.20	-0.01 ± 0.19
b_{22}	0.43 ± 0.31	0.04 ± 0.30	0.19 ± 0.17
c_{11}	-0.08 ± 0.11	-0.23 ± 0.09	-0.03 ± 0.15
c_{12}	-0.34 ± 0.09	-0.23 ± 0.15	-0.38 ± 0.14
c_{21}	0.08 ± 0.13	0.15 ± 0.10	-0.09 ± 0.17
c_{22}	0.22 ± 0.10	0.01 ± 0.17	0.25 ± 0.16
z_1	-0.050 ± 0.019	-0.024 ± 0.024	-0.011 ± 0.016
z_2	0.035 ± 0.017	-0.020 ± 0.041	0.011 ± 0.015
σ^2_{11}	0.053 ± 0.015	0.037 ± 0.008	0.195 ± 0.043

σ^2_{12}	-0.026 ± 0.008	-0.043 ± 0.012	-0.110 ± 0.032
σ^2_{22}	0.041 ± 0.010	0.103 ± 0.034	0.152 ± 0.034

†average of site-specific values

Table E2. Parameter estimates ± robust bootstrap standard errors for the taxonomic analysis.

Parameter†	Estimate ± rbse
a_1	-1.61 ± 0.29‡
a_2	-2.78 ± 0.33‡
a_3	-2.78 ± 0.32‡
a_4	-0.98 ± 0.16‡
a_5	-0.75 ± 0.11‡
a_6	-0.68 ± 0.10‡
b_{11}	0.19 ± 0.10
b_{22}	-0.08 ± 0.12
b_{33}	-0.09 ± 0.11
b_{44}	-0.09 ± 0.10
b_{55}	-0.15 ± 0.12
b_{66}	-0.06 ± 0.10
c_{11}	-0.45 ± 0.19
c_{12}	-0.93 ± 0.21
c_{21}	0.09 ± 0.18

c_{22}	0.26 ± 0.18
c_{31}	0.07 ± 0.07
c_{32}	0.11 ± 0.11
c_{41}	-0.27 ± 0.22
c_{42}	-0.04 ± 0.25
c_{51}	-0.08 ± 0.21
c_{52}	-0.03 ± 0.21
c_{61}	-0.05 ± 0.08
c_{62}	0.08 ± 0.13
z_1	-0.023 ± 0.019‡
z_2	0.073 ± 0.023‡
z_3	0.016 ± 0.018‡
z_4	0.008 ± 0.018‡
z_5	0.081 ± 0.011‡
z_6	0.003 ± 0.011‡
σ^2_{11}	0.718 ± 0.101
σ^2_{12}	0.053 ± 0.066
σ^2_{13}	0.013 ± 0.068
σ^2_{14}	0.066 ± 0.064
σ^2_{15}	0.112 ± 0.056
σ^2_{16}	0.068 ± 0.080

σ^2_{22}	0.897 ± 0.147
σ^2_{23}	0.175 ± 0.087
σ^2_{24}	0.202 ± 0.104
σ^2_{25}	0.103 ± 0.065
σ^2_{26}	-0.025 ± 0.090
σ^2_{33}	1.153 ± 0.230
σ^2_{34}	-0.032 ± 0.088
σ^2_{35}	0.074 ± 0.051
σ^2_{36}	-0.072 ± 0.053
σ^2_{44}	0.805 ± 0.151
σ^2_{45}	-0.020 ± 0.043
σ^2_{46}	-0.057 ± 0.053
σ^2_{55}	0.489 ± 0.168
σ^2_{56}	0.145 ± 0.123
σ^2_{66}	0.499 ± 0.141

† throughout, coral genera are coded as follows: 1: *Agarcia*, 2: *Diploria*, 3: *Montastrea*, 4: *Orbicella*, 5: *Porites*, 6: *Siderastrea*

‡ average of site-specific values

Sensitivities of long-run average cover with respect to each of the environmental factors are shown in Fig. E1. (Note that the sensitivities and trend shown in Fig. E1 are absolute sensitivities, and not proportional sensitivities as reported in the main text.) The figure shows that changes in each of the environmental factors (either an increase in average hurricane activity or seawater temperature, or the annual trend after accounting for hurricanes and sea temperature) would lead to an increase in macroalgal cover at the expense of both coral and "other" at both Tektite and Yawzi Point (although the effect of hurricanes on cover composition at Tektite appears to be minimal). At the RS, increases in average seawater temperature would decrease both macroalgal and coral cover.

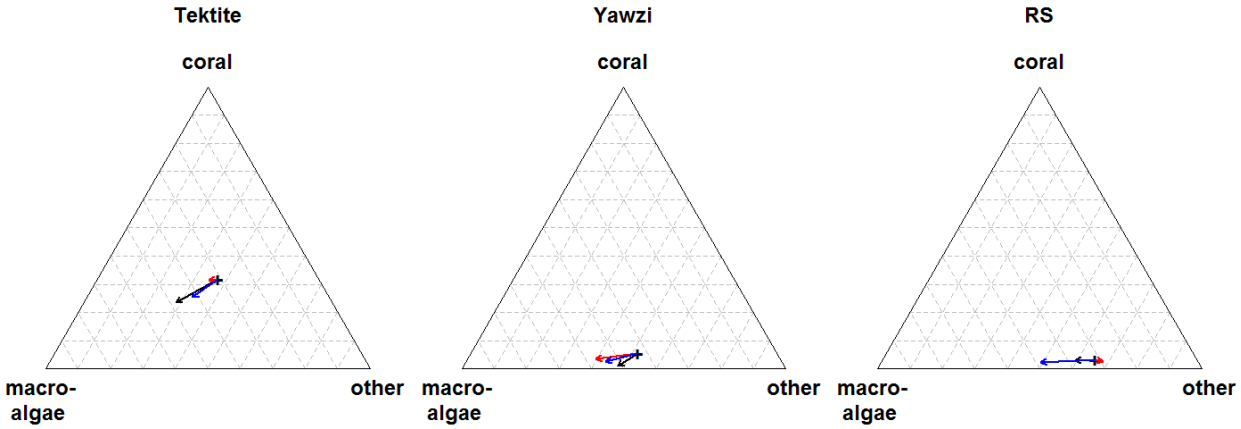

Figure E1. Sensitivity (i.e., $d\boldsymbol{\mu}_p / d\boldsymbol{\mu}_u$) and trend (i.e., $d\boldsymbol{\mu}_p / dt^*$) of the entire cover composition at three habitats. In each panel, the plus sign denotes the metric center of the 2012 quasi-stationary distribution. Red, blue and black arrows show sensitivity of cover composition with respect to hurricane activity, seawater temperature, and the annual trend respectively. To make arrows more visible, the length of each arrow corresponds to the rate of change of

the cover calculated with respect to 1 additional hurricane per year, 1 additional DHM per year, or to 10 additional years.

Sensitivities of the SD of coral cover to the SD of each of the random environmental factors are shown in Figure E2. Sensitivities are calculated assuming that the (product-moment) correlation between hurricane activity and DHMs remains fixed. That is, an increase in the SD of one environmental factor also increases the covariance between the two random environmental factors. Error bars in fig. E2 are ±1 robust bootstrap s.e. However, in most cases the bootstrap sampling distributions are severely right skewed, such that a bootstrap-based confidence interval would not be symmetric around the point estimate. For reference, the SD of hurricane activity for 1992 – 2012 was 0.55, and the SD of DHM was 0.46.

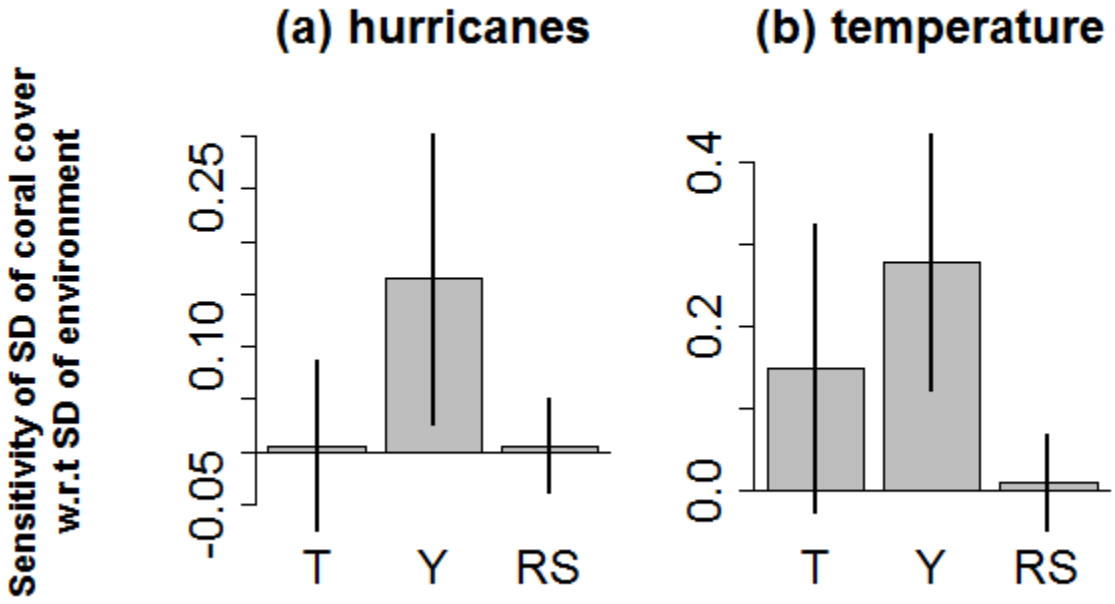

Figure E2. Sensitivity (i.e., $d\sigma_{\mathrm{p}}/d\sigma_{\mathrm{u}}$) of the SD of long-run coral cover with respect to the SD of (a) annual hurricane activity and (b) annual DHM at Tektite (T), Yawzi Point. (Y), and the random sites (RS). Sensitivities are calculated with respect to a 100% increase in the SD of the environmental covariate. Error bars are ±1 robust bootstrap s.e.